JOURNAL OF SPACECRAFT AND ROCKETS
Vol. 34, No. 4, July–August 1997

Aerodynamic Characteristics Evaluation of Hypersonic Flight Experiment Vehicle Based on Flight Data

Shigeya Watanabe,* Shinji Ishimoto,† and Yukimitsu Yamamoto‡
National Aerospace Laboratory, Tokyo 182, Japan

A hypersonic flight experiment was conducted for development of the Japanese unmanned operational orbiting plane. The following aerodynamic characteristic data are presented for a flight ranging in Mach number from 2 to 14: aerodynamic force coefficients, longitudinal trim characteristics, stability and control derivatives, elevon hinge moment, and surface pressure distribution. The data are compared with preflight predictions based on wind-tunnel test results and computational fluid dynamic calculations to evaluate the validity of the prediction methods, including determination of uncertainty in the vehicle design. The prediction methods are proven to be generally valid for design of lifting re-entry vehicles at a high angle of attack, whereas some anomalies are found in axial force, elevon trim angle, and reaction-control-system gas-jet interaction.

Nomenclature

b	= body width, m
C_A	= axial force coefficient, F_A/qS
C_{A_F}	= forebody axial force coefficient, $C_A + C_{p_B} S_B/S$
C_l	= rolling moment coefficient, l/qSb
C_{mH}	= elevon hinge moment coefficient, $m_e/qS_e l_e$
C_N	= normal force coefficient, F_N/qS
C_n	= yawing moment coefficient, n/qSb
C_p	= pressure coefficient, $(p - p_\infty)/q$
C_{p_B}	= base pressure coefficient, $(p_B - p_\infty)/q$
C_∞	= Chapman–Rubesin constant, $\mu_w T_\infty/\mu_\infty T_w$
F	= force, N
L/D	= lift-to-drag ratio
l, m, n	= rolling, pitching, and yawing moment, N-m
l_B	= body length, m
l_e	= length of elevon, m
M	= freestream Mach number
p	= pressure, Pa
q	= dynamic pressure, Pa
Re_{l_B}	= freestream Reynolds number based on body length
S	= planform area, m^2
S_B	= body base area, m^2
S_e	= area of elevon, m^2
T	= temperature, K
$\bar{V}_\infty$	= viscous interaction parameter, $M\sqrt{(C_\infty/Re_{l_B})}$
X, Y, Z	= coordinates fixed to vehicle, m (see Fig. 1)
X_{CP}	= X coordinate of center of pressure, m
α	= angle of attack, deg
β	= angle of sideslip, deg
Δ	= uncertainty
ΔC_{Av}	= estimated axial force coefficient increment due to viscous interaction effect
δ_a	= elevon deflection angle as aileron, deg $(\delta_L - \delta_R)/2$
δ_e	= elevon deflection angle as elevator, deg $(\delta_L + \delta_R)/2$
μ	= coefficient of viscosity, kg/(s-m)

Subscripts

B	= condition on body base
CG	= vehicle center of gravity
e	= elevon
w	= condition on wall
β, δ_a	= partial derivatives with respect to subscripted variables
∞	= freestream condition

Received Sept. 3, 1996; presented as Paper 96-4527 at the 7th International Space Planes and Hypersonic Systems and Technologies Conference, Norfolk, VA, Nov. 18–22, 1996; revision received March 14, 1997; accepted for publication March 25, 1997.

*Senior Researcher, Aerodynamics Division, 7-44-1 Jindaiji-higashi-machi, Chofu. Member AIAA.

†Researcher, Flight Research Division, 7-44-1 Jindaiji-higashi-machi, Chofu. Member AIAA.

‡Laboratory Head, Aerodynamics Division, 7-44-1 Jindaiji-higashi-machi, Chofu. Member AIAA.

Introduction

SEVERAL experimental hypersonic lifting vehicles such as ASSET and PRIME (X-23A) were developed in the 1960s and 1970s to acquire real-flight data in hypersonic speed, which were used for the aerodynamic design of the Space Shuttle Orbiter. Various aerodynamic data obtained in the Space Shuttle flights were compared extensively with preflight predictions based on wind-tunnel test data, leading to some improvements in the aerodynamic characteristic estimation technique.[1] However, since the Space Shuttle, new hypersonic flight data useful for validating recent advanced computational fluid dynamics (CFD) have not been obtained.

The hypersonic flight experiment (HYFLEX) project[2] was planned as one of a series of small-scale experimental vehicles for development of the Japanese unmanned, operational orbiting plane, H-II orbiting plane (HOPE). The purpose of the HYFLEX project was to acquire hypersonic flight data on aerodynamics, a thermal protection system, and guidance and control. The experiment was successfully performed,[3] and various flight data were transmitted by telemetry to the ground during the entry flight.

The purpose of this paper is to evaluate the ground-based aerodynamic characteristic prediction methods applied in the HYFLEX vehicle design by comparing the flight data and preflight predictions based on wind-tunnel test results and CFD calculations. The following aerodynamic data are presented in the super- to hypersonic speed range: 1) aerodynamic force and moment, 2) stability and control derivatives including aerodynamic effectiveness of the aerodynamic control surface, termed elevon, 3) elevon hinge moment, and 4) surface pressure distribution. The reasons for discrepancies are discussed to improve the accuracy of current prediction methods.

Preflight Prediction Method

Wind-Tunnel Tests

To predict aerodynamic characteristics of the HYFLEX vehicle, wind-tunnel tests and CFD calculations were performed for flight configuration HRV03-540 shown in Fig. 1 and the previous configuration, HRV03-530. The difference between the configurations is that HRV03-530 is without a forebody upper surface bulge. Reference dimensions to nondimensionalize the measured aerodynamic data are shown in Table 1.

Six components of aerodynamic force and moment and stability and control derivatives were predicted on the basis of the wind-tunnel test results covering a Mach number range from 2 to 10. Hinge moments of the elevons were also measured in the tests. The data were used as basic aerodynamic characteristics in the vehicle system design.

Table 2 summarizes the wind tunnels used and the test conditions. In Fig. 2, the wind-tunnel test ranges of the freestream Reynolds number, viscous interaction parameter, angle of attack, and angle of sideslip are compared with the actual flight ranges of HYFLEX. In the region where aerodynamic force has a significant effect on the flight, the tests almost cover the flight range of all parameters except Mach number and the viscous interaction parameter. Above Mach 10, Mach number effects are assumed to be negligible. Between Mach 4 and 10, aerodynamic characteristics are interpolated according to Mach number dependency in the case of the Space Shuttle Orbiter. The angle of attack in the flight was kept almost constant except for a gradual pitch-down maneuver from Mach 11 to 8 and a sudden pitch down at Mach 2.9. All of the preflight predictions presented were calculated along the angle-of-attack profile in the actual flight shown in Fig. 2.

The ONERA S4MA hypersonic wind tunnel was used to acquire force and moment data in the hypersonic speed range. Validity of the data was confirmed by Newtonian flow calculations and CFD. The National Aerospace Laboratory hypersonic wind tunnel (NAL HWT) and shock tunnel (NAL SHKT) were also used for surface-pressure distribution measurement in the hypersonic speed range. Three wind tunnels were used for investigating supersonic characteristics: the high-speed wind tunnel at Fuji Heavy Industries (FHI HSWT), the supersonic wind tunnel in the Institute of Space and Astronautical Science (ISAS SWT), and the NAL supersonic wind tunnel (NAL SWT). The data were compared to certify uncertainty in the measurements.

In the case of the Space Shuttle,[4] to define the uncertainty of the predicted value, many wind-tunnel tests for the Orbiter were conducted in many different wind tunnels by using different models. As a result, tolerance, which means variation of data among different wind tunnels, was determined. Wind-tunnel data and flight data for some aircraft were also extensively examined previously, leading to variation, which means the effects on aerodynamics due to differences between wind-tunnel condition and flight condition. In the case of HYFLEX vehicle development, we could use only a few wind tunnels for a speed range, and the test cases were highly restricted because of low availability of wind tunnels and a tight development schedule. Therefore, we defined measurement error of each individual wind tunnel instead of tolerance. The measurement error consists of a force balance error, wind-tunnel freestream condition errors, an error due to misalignment of the model, and so forth. As Japan did not have any flight data of lifting hypersonic vehicles in the past, the variation for HYFLEX was estimated on the basis of the variation of the Space Shuttle. We transformed the Space Shuttle variation into the HYFLEX variation, assuming that aerodynamic force and moment variations of both vehicles with the same planform area were the same. The magnitude of measurement error was larger than 20% of the magnitude of the variation in most cases and in a few cases was larger than the variation. To take account of the significant measurement error, uncertainty of the prediction was defined as the root sum square of the measurement error and the variation. All of the uncertainties of the preflight predictions shown denote a 3σ level (99.7% odds).

Table 1 Reference dimensions of HYFLEX vehicle

Reference area S	4.270 m^2
S_B	0.931 m^2
Longitudinal reference l_B	4.000 m
Lateral/directional reference b	1.200 m
Moment reference center (center of gravity)	
X_{CG} (57.5% l_B)	2.3001 m
Y_{CG}	0.0007 m
Z_{CG}	0.4315 m
Reference area for hinge moment S_e	0.1677 m^2
Reference length for hinge moment l_e	0.400 m
Moment reference center of hinge moment X_e	4.025 m

Table 2 Wind tunnels and test conditions

Name	Nozzle exit size, m	Test Mach range	Measurement items[a]				Model configuration
			F/M	H/M	S/P	F/V	
ONERA S4MA	ϕ0.99	9.9	√	√		√	HRV03-530
NAL HWT	ϕ1.27	10.0–10.1			√	√	HRV03-540
NAL SHKT	ϕ0.44	9.7–10.3			√		HRV03-540
FHI HSWT	0.61 × 0.61	0.5–3.9	√			√	HRV03-530
ISAS SWT	0.60 × 0.60	1.6–4.0	√	√		√	HRV03-530
NAL SWT	1.00 × 1.00	2.0–4.0			√	√	HRV03-540

[a] F/M, six components of force and moment; H/M, elevon hinge moment; S/P, surface pressure; F/V, flow visualization (schlieren, shadow graph, or oil flow).

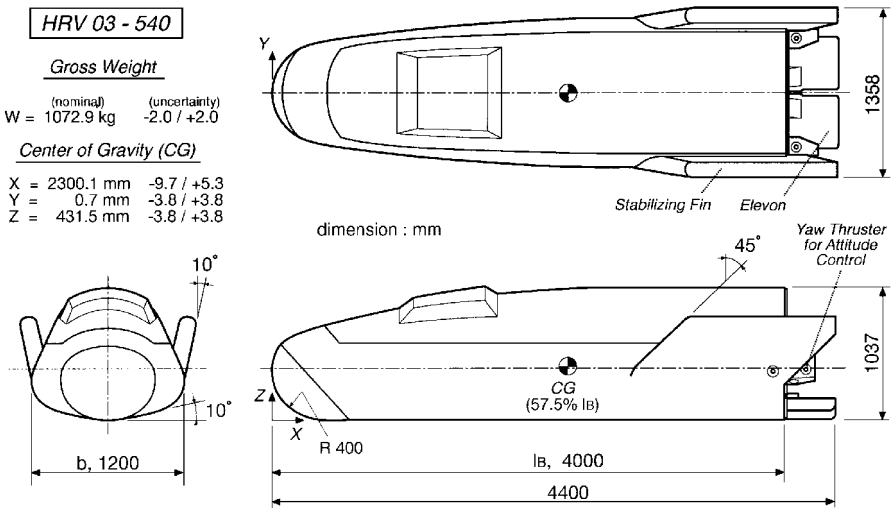

Fig. 1 HYFLEX vehicle configuration.

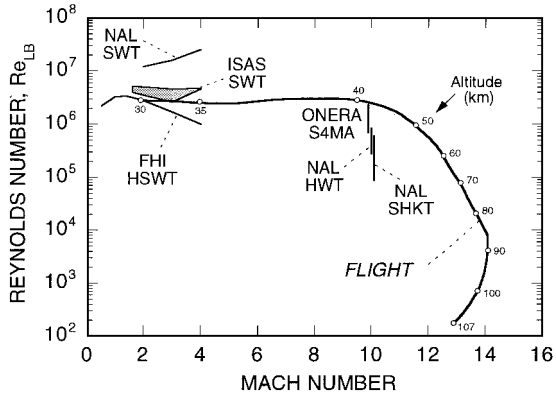

Freestream Reynolds number

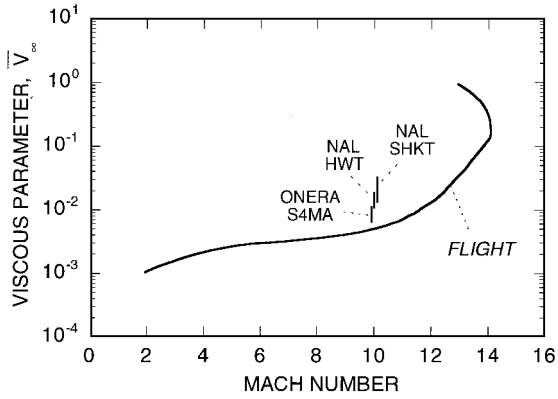

Viscous interaction parameter

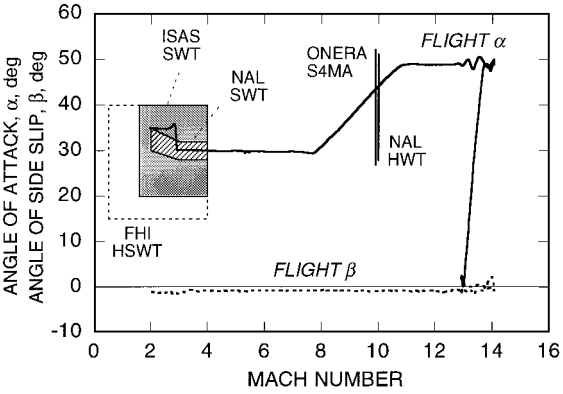

Angle of attack and sideslip angle

Fig. 2 Flight condition and vehicle attitude.

CFD Calculations

CFD calculations using a Navier–Stokes code were conducted to confirm validity of the wind-tunnel test results and to determine surface-pressure distribution for design of the vehicle structure.[5] In most of the calculations, perfect gas was assumed because total enthalpy during the HYFLEX flight was not high enough to generate a significant real gas effect on aerodynamic characteristics. In some cases, to estimate a real gas effect on aerodynamic heating and aerodynamic characteristics, nonequilibrium flow with a noncatalytic wall was assumed. A boundary layer was assumed to be laminar on the whole vehicle surface because the estimated maximum Reynolds number in the flight was considered to be lower than a predicted transition Reynolds number.

Reduction of Flight Data

Aerodynamic force coefficients—that is, normal, axial, and side force coefficients—are directly reduced from three-axis acceleration data measured by three accelerometers installed in an onboard inertial measurement unit. To eliminate noise from the 40-Hz sampling accelerometer outputs, the outputs are averaged in a time span of 1 s.

Table 3 Uncertainties of flight measurement data

	Uncertainty				
M	ΔC_N	ΔC_A	$\Delta L/D$	$\Delta\delta_e$, deg	ΔC_{mH}
2.99	±0.034	±0.012	±0.068	±0.5	±0.030
7.14	±0.031	±0.006	±0.044	±0.5	±0.012
12.07	±0.039	±0.008	±0.034	±0.5	±0.026

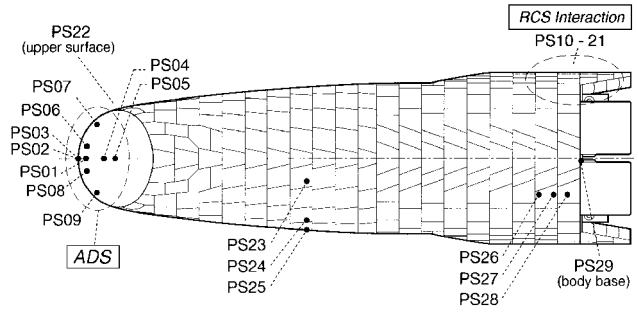

Fig. 3 Location of surface-pressure measurement ports.

The maximum-likelihood (ML) method based on the Illif–Maine formulation[6] is used to extract the stability and control derivatives and moment generated by yaw reaction-control-system (RCS) thrusters from vehicle motion in flight. The ML estimator minimizes a cost function, which indicates the differences between the measured and computed attitude responses. The motion of the vehicle is computed by a linear time-independent state-space model. The ML estimator also provides a measure of the reliability of estimated parameters. The measure, also termed the Cramer–Rao bound or the uncertainty level, indicates an approximate standard deviation of a parameter.

To measure hinge moments of the elevons, strain gauges were installed on right and left elevon-actuating link rods. On the basis of stress outputs, the moments around elevon hinges were reduced. Hinge moments due to aerodynamic force alone were extracted with correction of inertial force contribution due to vehicle acceleration. Note that the correction is important for obtaining accurate hinge moments because the acceleration normal to the vehicle X axis reaches 5.6 g during the entry flight.

As shown in Fig. 3, surface pressure was measured at 29 points located on the whole vehicle surface exclusive of elevon surface. Data at eight points, PS22-29, are for measurement of general surface-pressure distribution on the vehicle, whereas others are for the air data sensor and RCS gas-jet interaction experiments.

Atmospheric properties needed for nondimensionalizing the measured aerodynamic force and moment were estimated from remote sensing atmospheric temperature data obtained by the National Oceanic and Atmospheric Administration (NOAA) polar-orbiting satellite on the day of the flight. The estimation method was validated four times before the flight in comparison with the data directly measured by sounding rockets launched in Japan. The results showed that at an altitude of less than 55 km, the root mean square of the differences in pressure and temperature was less than 3% and 10 K, respectively.[7] On the other hand, the pressure difference between the sounding rocket data and the U.S. standard atmosphere model 1976 is more than 10% above an altitude of 45 km. The results obviously indicate the advantage of the estimation method based on the NOAA data relative to the U.S. standard atmosphere.

Table 3 shows uncertainties of flight measurement data at three Mach numbers. The uncertainties were calculated considering the accuracy of sensors, the resolution of A/D transformation, and dynamic pressure estimation uncertainty. Here, the uncertainty of dynamic pressure estimated on the basis of the NOAA data was assumed to be 3% throughout the flight, based on comparison with the sounding rocket data.

Comparisons of Flight Data with Preflight Predictions

Aerodynamic Force Coefficients

Figure 4 shows comparisons of the normal-force coefficient C_N and the axial-force coefficient C_A between flight data and

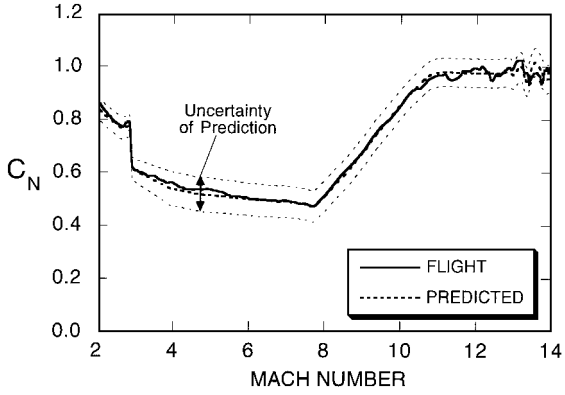

a) Normal-force coefficient

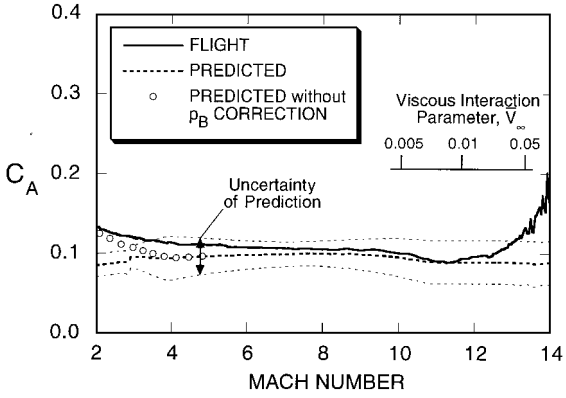

b) Axial-force coefficient

Fig. 4 Longitudinal force coefficient comparison.

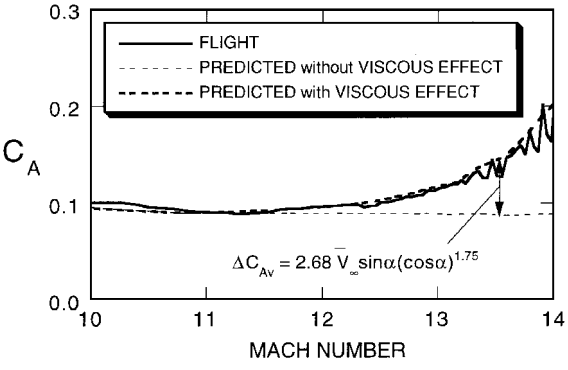

Fig. 5 Viscous interaction effects on axial-force coefficients.

predictions. The predicted values are calculated for Mach number, angle of attack, and elevon deflection angle in flight. In the whole Mach number range, the flight C_N value agrees well with the prediction within uncertainty. Variation of the flight C_N value above Mach 11 is considered to be due to error of the dynamic pressure estimation because such variation is not observed in L/D.

Difference in C_A between the flight data and the prediction is less than the uncertainty in a Mach number range from 4 to 13. However, the flight C_A value is much greater than the prediction below Mach 4 and above Mach 13. The discrepancy in the high Mach number range seems to be a viscous interaction effect as observed in the Space Shuttle flight.[8,9] Figure 5 shows a predicted C_A with the viscous interaction effect correction, which was proposed for the Space Shuttle Orbiter.[9] In the correction, the difference in the ratio of the lower surface wetted area to the reference area between the HYFLEX vehicle and the Space Shuttle Orbiter is taken into account. The prediction with the viscous effect correction agrees well with the flight data in spite of the configuration difference between the HYFLEX vehicle and the Space Shuttle Orbiter. This agreement means that this viscous effect correction method is promising for various re-entry vehicle configurations with a high angle of attack.

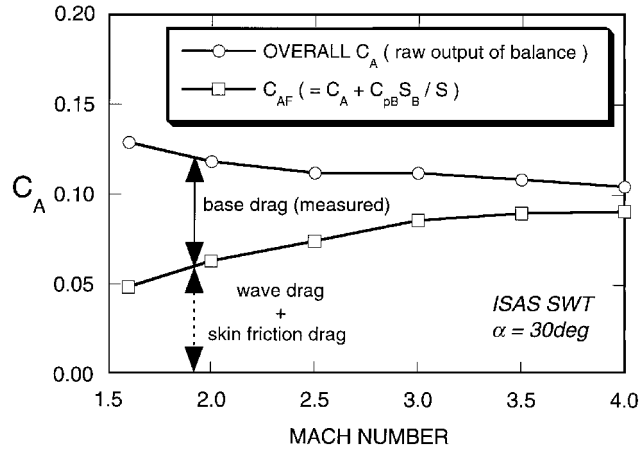

Fig. 6 Axial-force coefficients in wind-tunnel tests.

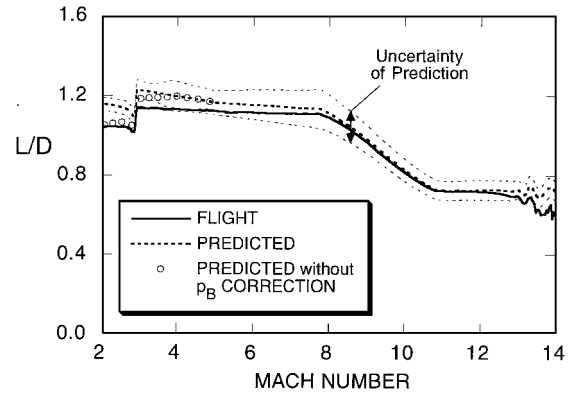

Fig. 7 *L/D* comparison.

As explained in detail, the cause of the C_A difference below Mach 4 is an improper base pressure measurement in the supersonic wind-tunnel tests. In the prediction, the flight C_A value is estimated as a sum of forebody drag based on the wind-tunnel test data and in-flight base drag estimated from a base pressure correlation based on some turbulent axisymmetric body experiments without sting support interference.[10] This prediction method of C_A is adopted for eliminating the support sting interference effect on base pressure in the wind-tunnel tests. Figure 6 shows axial force data acquired in a supersonic wind-tunnel test. Presented are overall C_A values reduced from a raw output of a force balance and forebody axial force coefficient C_{A_F}, with the base drag correction based on measured base pressure. The reduced C_{A_F}, which decreases with a decrease in Mach number, is obviously wrong because the wave drag, which is dominant in C_{A_F}, should increase with a decrease in Mach number in a low supersonic speed range. We conclude that the base pressure measurement method where pressure data at four points close to the support sting are averaged is inaccurate because significant base pressure variation on the base area may exist with a high angle of attack. If C_A without the base pressure correction in the wind-tunnel tests is used as a predicted value, agreement between the flight and the prediction improves as shown in Fig. 4b, although the sting interference effect is included in the predicted C_A.

Figure 7 shows a comparison of L/D. In the case of the wind-tunnel test data without the base pressure correction, agreement between flight and prediction is good below Mach 12, whereas the flight L/D is a little smaller than the prediction below Mach 8. The difference above Mach 12 is due to the viscous interaction effect as already mentioned.

Longitudinal Trim Characteristics

The elevon deflection angle as an elevator δ_e for longitudinal trim is shown in Fig. 8. The predicted value is a deflection angle in static trim condition, assuming pitch maneuver of the vehicle is quasistatic throughout the flight. Uncertainty of δ_e in the trim condition includes pitching-moment coefficient uncertainty alone,

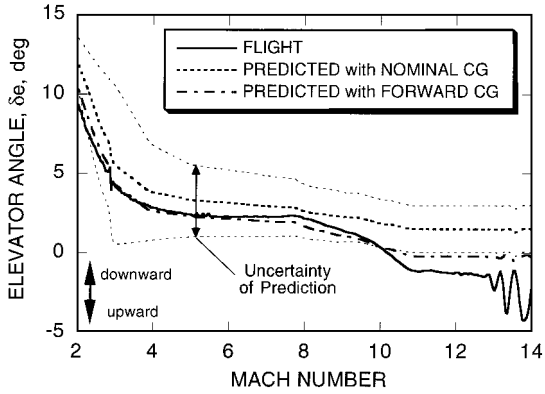

Fig. 8 Longitudinal trim comparison.

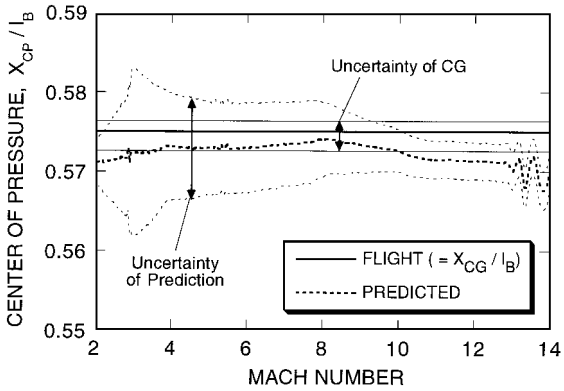

Fig. 9 Center of pressure location comparison.

excluding the uncertainty of location of the center of gravity. Below Mach 8, flight δ_e is a little lower—that is, upward deflection—than the predicted deflection angle. It is inferred that the causes are a measurement error of the center of gravity and a nose-down moment generated by the forebody upper surface bulge, which was not simulated in the hypersonic wind-tunnel test model configuration used to acquire the prediction data. As shown in Fig. 8, agreement between flight data and prediction is better with a forward center of gravity, considering uncertainty in the measurement of the center of gravity location (see Fig. 1). Above Mach 10, the difference between the flight δ_e and the prediction is beyond uncertainty. The cause of the large difference is not known, but some reasons such as support sting interference in the wind-tunnel tests and a real gas effect are being investigated in addition to the causes already mentioned. Above Mach 13, deflection of the elevon in flight is slightly upward to compensate for the nose-down moment caused by a skin friction increase on the lower surface because of the viscous interaction effect.

Figure 9 shows a comparison of center of pressure locations. It is assumed that the center of pressure in flight coincided with the center of gravity because the pitch maneuver was almost quasistatic during flight. Moreover, the change in the center of gravity position during flight was negligibly small, which led to a constant center of pressure location throughout the flight as shown. The predicted center of pressure is more forward than that in flight. The maximum difference is about 0.4% l_B around Mach 12.

Stability and Control Derivatives

Lateral and directional stability derivatives with respect to sideslip angle and control derivatives with respect to aileron deflection angle are shown in Figs. 10 and 11, respectively. All of the identified derivatives based on the motion in flight agree with predicted values within uncertainty. The agreement proves that the prediction based on the wind-tunnel tests and the method determining uncertainty are valid.

Because any special maneuvers useful for longitudinal derivative identification were not performed in the HYFLEX flight, identification of longitudinal derivatives was impossible except for a high-rate pitch-up maneuver at Mach 2.9.

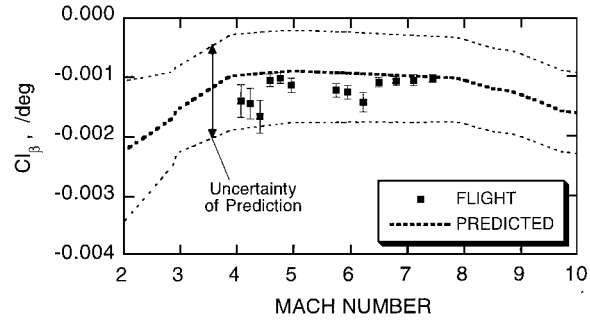

Rolling moment derivative

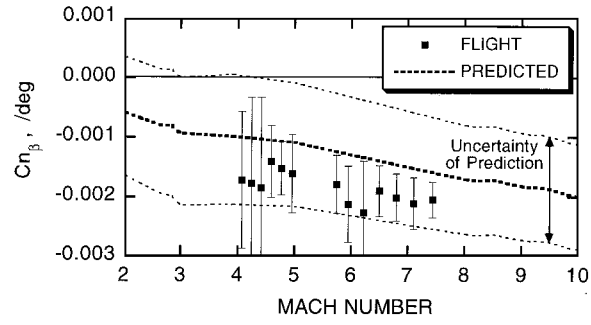

Yawing moment derivative

Fig. 10 Lateral/directional stability derivative comparison.

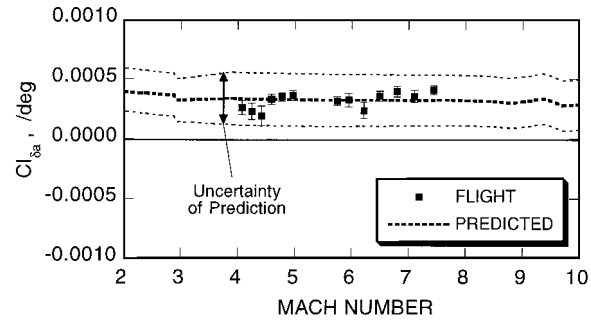

Rolling moment derivative

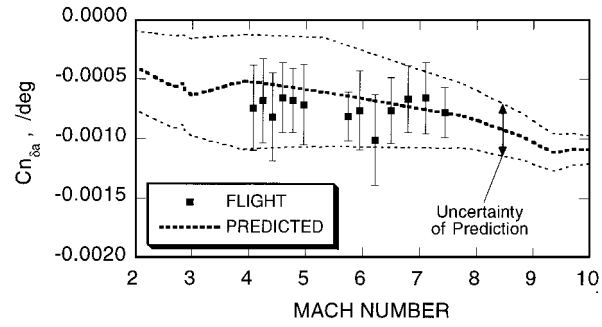

Yawing moment derivative

Fig. 11 Lateral/directional control derivative comparison.

Figure 12 shows rolling and yawing moments due to injections of the left yaw RCS gas jet for attitude control. As shown in Fig. 1, the gas-jet thruster is located on a left RCS thruster bulge mounted on the body base, and the position in the Z direction is a little lower than the center of gravity. The direction of the jet is perpendicular to the vehicle symmetrical plane, so the thrust in a vacuum generates a negative yawing moment and a small negative rolling moment, as shown in Fig. 12. Compared with the moments generated by the jet nozzle thrust in a vacuum, magnitudes of both rolling and yawing moments in flight are much larger because of gas-jet interaction with

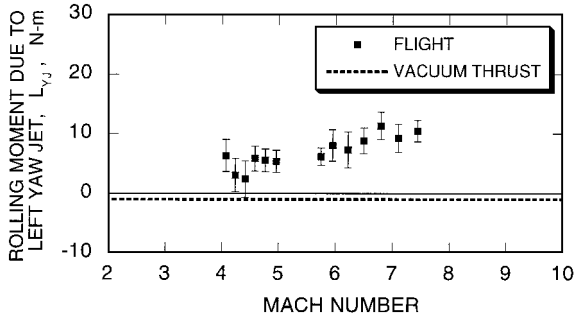

Rolling moment

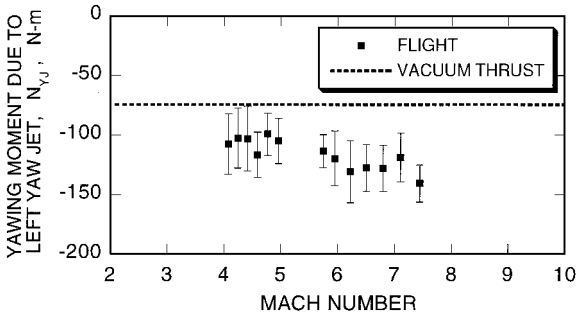

Yawing moment

Fig. 12 Rolling and yawing moment due to yaw RCS jet injection.

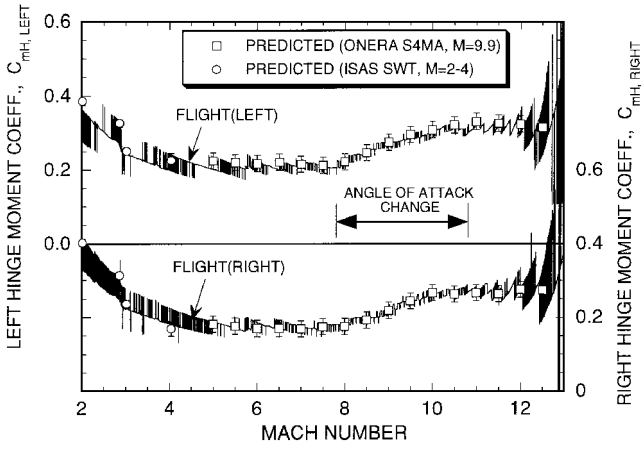

Fig. 13 Elevon hinge moment comparison.

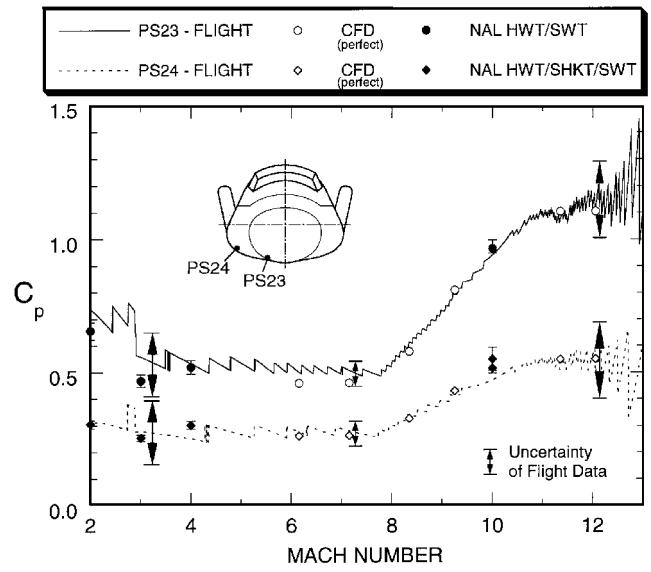

Fig. 14 Body lower surface-pressure comparison.

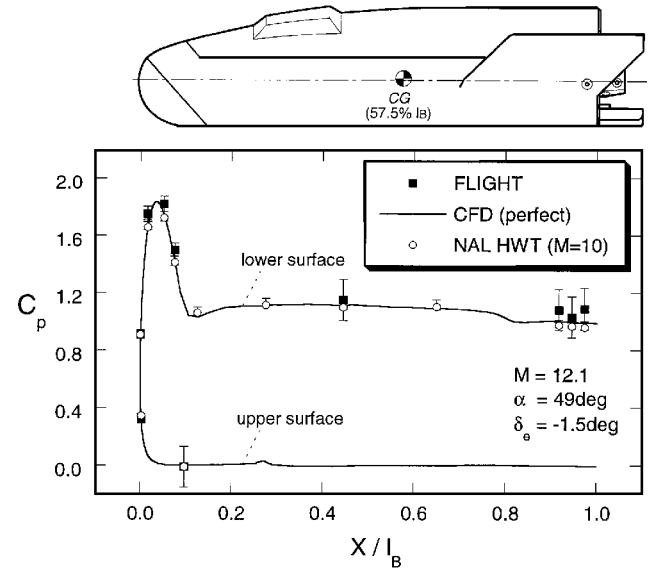

Fig. 15 Vehicle center line surface-pressure comparison.

external flow. This result coincides with the fact that increases in pressure were observed at the jet injection timing on the upper, rear part of the left stabilizing fin in flight pressure measurements (PS14, -15, and -19) (Ref. 7) and that total impulse of the yaw RCS in flight was much less than the estimated value in the vehicle design where the interaction effect was not considered.[11] The interaction effect on rolling and yawing moments was also observed in a postflight hypersonic wind-tunnel test to investigate the RCS gas-jet interaction phenomena.

Elevon Hinge Moments

Comparisons of elevon hinge moment coefficients are presented in Fig. 13. The wind-tunnel test data at Mach 9.9 are used as predicted values above Mach 5 regardless of Mach number dependency. Agreement between the flight data and the prediction is good, especially above Mach 5. Note that Mach number effects on the hinge moments are very small above Mach 5, as evidenced from the fact that the prediction based on the test data at Mach 9.9 is valid in the Mach number range.

Surface Pressure

Surface pressure on the middle of the lower body surface, PS23 and -24, is shown in Fig. 14 compared with predictions based on several wind-tunnel test results and CFD calculations assuming a perfect gas. The predictions are judged to be reasonable, whereas resolution of the flight-measured pressure is insufficient for a precise comparison, especially in a supersonic speed range.

Figure 15 compares surface-pressure distribution nearly on the center line of the vehicle at Mach 12.1 with an angle of attack of 49 deg. The surface-pressure distribution in flight is reasonably simulated by the predictions based on a wind-tunnel test and a CFD calculation.

Concluding Remarks

Some comparisons of the HYFLEX aerodynamic characteristics between flight data and preflight predictions have been presented. The results indicate that the prediction methods based on wind-tunnel test results and CFD calculations were generally valid in the super- to hypersonic speed range for hypersonic high-angle-of-attack re-entry vehicle design. We also confirmed that the method determining the uncertainty of the predictions was reasonable in spite of a small amount of wind-tunnel test data.

However, some anomalies were found. 1) Axial force was underestimated by the preflight prediction because of elimination of a viscous interaction effect and an inaccurate base pressure measurement. 2) Elevon trim angle in flight was lower than predicted. 3) Fairly strong yaw-jet interaction effects on rolling and yawing moments were observed.

Acknowledgments

The wind-tunnel tests in the vehicle design phase were conducted by the HYFLEX Joint Team, which consisted of the National Aerospace Laboratory (NAL), the National Space Development Agency of Japan, and various contractors. The wind-tunnel tests in NAL were performed with the help of members of the NAL supersonic and hypersonic wind-tunnel facilities/instrumentations laboratories. The test in the Institute of Space and Astronautical Science was supported by Yoshifumi Inatani and Motoyuki Hongo. The authors would like to express their appreciation for the efforts and support by all persons who took part in these tests.

References

[1]Maus, J. R., Griffith, B. J., Szema, K. Y., and Best, J. T., "Hypersonic Mach Number Effects and Real Gas Effects on Space Shuttle Orbiter Aerodynamics," *Journal of Spacecraft and Rockets*, Vol. 21, No. 2, 1984, pp. 136–141.

[2]Shirouzu, M., and Watanabe, S., "On the Hypersonic Flight Experiment (HYFLEX) for the Development of HOPE," AIAA Paper 93-5080, Nov. 1993.

[3]Shirouzu, M., Watanabe, S., and Suzuki, H., "A Quick Report of the Hypersonic Flight Experiment, HYFLEX," *Twentieth International Symposium on Space Technology and Science (ISTS)*, Paper 96-f-09, May 1996.

[4]Young, J. C., and Underwood, J. M., "Development of Aerodynamic Uncertainties for the Space Shuttle Orbiter," *Journal of Spacecraft and Rockets*, Vol. 20, No. 6, 1983, pp. 513–517.

[5]Yamamoto, Y., Wada, Y., and Yoshioka, M., "HYFLEX Computational Fluid Dynamic Analysis; Part II," AIAA Paper 95-2274, June 1995.

[6]Illif, K. W., and Shafer, M. F., "Extraction of Stability and Control Derivatives from Orbiter Flight Data," NASA TM-4500, June 1993.

[7]Inouye, Y., Fujii, K., Takizawa, M., Takaki, R., Watanabe, S., and Ito, T., "Flight Results of HYFLEX Onboard Measurements," AIAA Paper 96-4528, July 1996.

[8]Romere, P. O., Kanipe, D. B., and Young, J. C., "Space Shuttle Entry Aerodynamic Comparisons of Flight 1 with Preflight Predictions," *Journal of Spacecraft and Rockets*, Vol. 20, No. 1, 1983, pp. 15–21.

[9]Griffith, B. J., Maus, J. R., and Best, J. T., "Explanation of the Hypersonic Longitudinal Stability Problem—Lessons Learned," NASA CP-2283, Pt. 1, March 1983, pp. 347–379.

[10]Jorgensen, L. H., "Prediction of Static Aerodynamic Characteristics for Space-Shuttle-Like and Other Bodies at Angles of Attack from 0° to 180°," NASA TN D-6996, Jan. 1973.

[11]Ishimoto, S., Takizawa, M., Suzuki, H., and Morito, T., "Flight Control System of Hypersonic Flight Experiment Vehicle," AIAA Paper 96-3403, July 1996.

J. C. Adams Jr.
Associate Editor